Supplementary Material for Journal of Materials Chemistry A.

Fabrication of CuO_x nanowires@$NiMnO_x$ nanosheets core@shell-type electrocatalysts: crucial roles of defect modification and valence state for overall water electrolysis

Suchada Sirisomboonchai[a], Xiumin Li[b], Nutthaphak Kitiphatpiboon[a], Rinrada Channoo[c,d], Shasha Li[e], Yufei Ma[f], Suwadee Kongparakul[d], Chanatip Samart[d], Abuliti Abudula[a], Guoqing Guan[a,c,*]

[a.] *Graduate School of Science and Technology, Hirosaki University, 1-Bunkyocho, Hirosaki 036-8560, Japan.*

[b.] *School of Materials Science and Engineering, Zhengzhou University, Zhengzhou 450001, China.*

[c.] *Energy Conversion Engineering Laboratory, Institute of Regional Innovation (IRI), Hirosaki University, 2-1-3, Matsubara, Aomori 030-0813, Japan. *e-mail: guan@hirosaki-u.ac.jp*

[d.] *Department of Chemistry, Faculty of Science and Technology, Thammasat University, Pathumtani 12120 Thailand*

[e.] *College of Chemical and Biological Engineering, Taiyuan University of Science and Technology, Taiyuan 030024, China.*

[f.] *School of Chemical Engineering and Light Industry, Guangdong University of Technology, Guangzhou 510006, China*

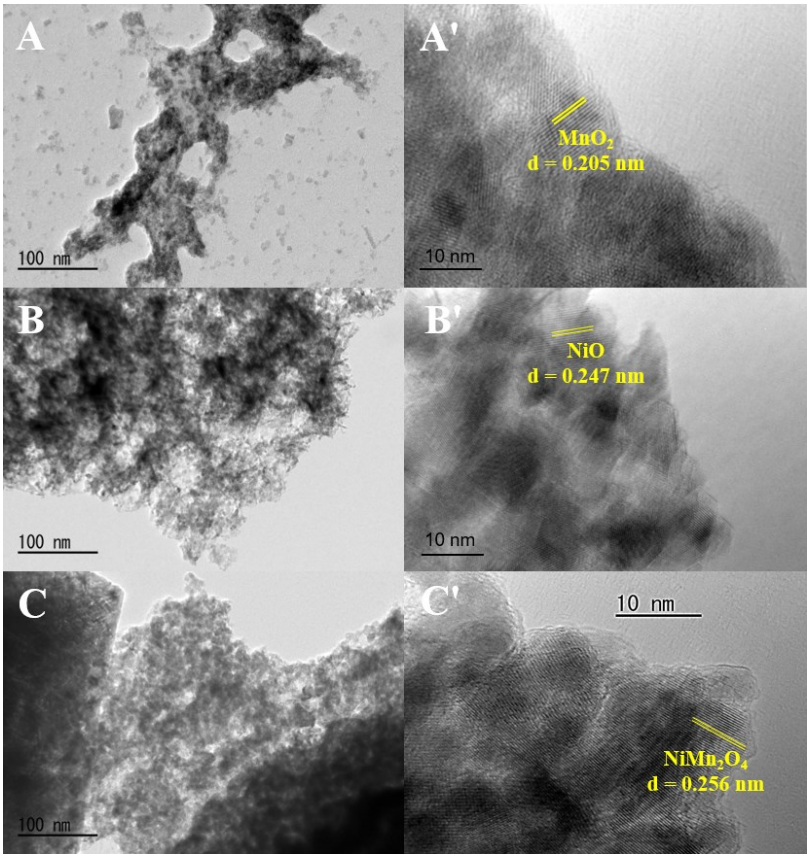

Figure S1. TEM images of (A, A') MnO_x, (B, B') NiO, and (C, C') $NiMnO_x$ NSs.

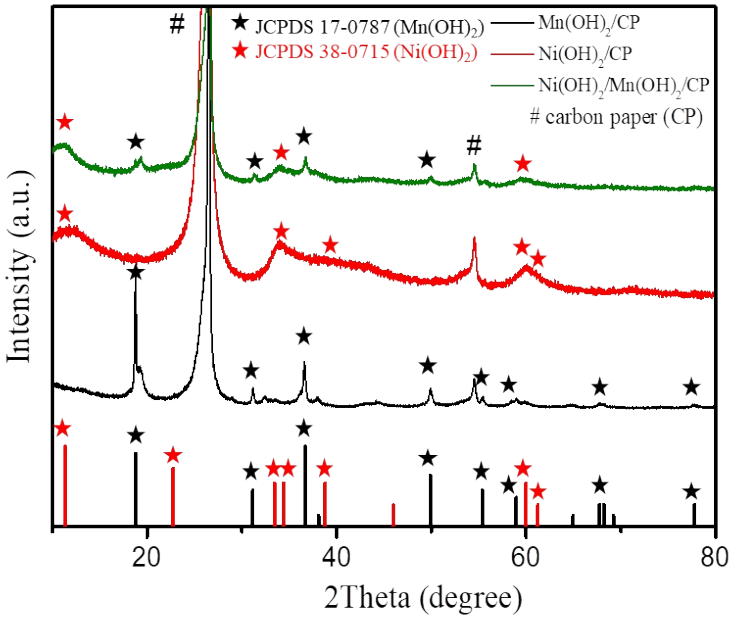

Figure S2. (A) XRD patterns of $Mn(OH)_2$/CP, $Ni(OH)_2$/CP and $Mn(OH)_2$/$Ni(OH)_2$/CP composite.

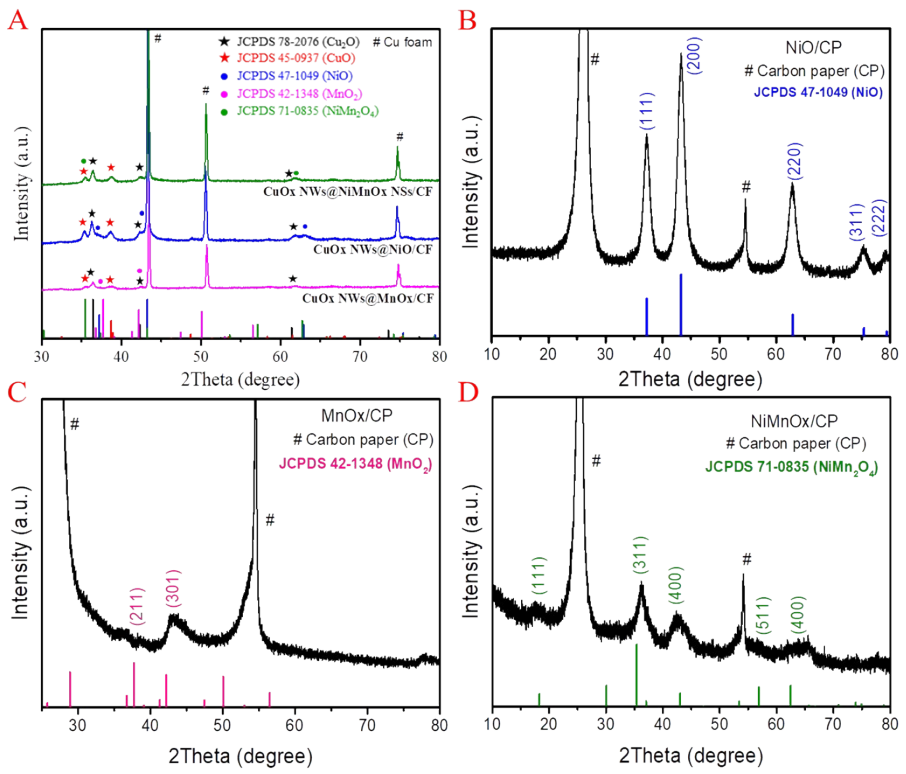

Figure S3. (A) XRD patterns of CuO_x NWs@MnO_x/CF, CuO_x NWs@NiO/CF, CuO_x NWs@$NiMnO_x$ NSs/CF. (B-D) XRD pattern of catalysts deposited on carbon paper (CP) substrate (D) NiO/CP (C) MnO_x/CP (D) $NiMnO_x$ NSs/CP.

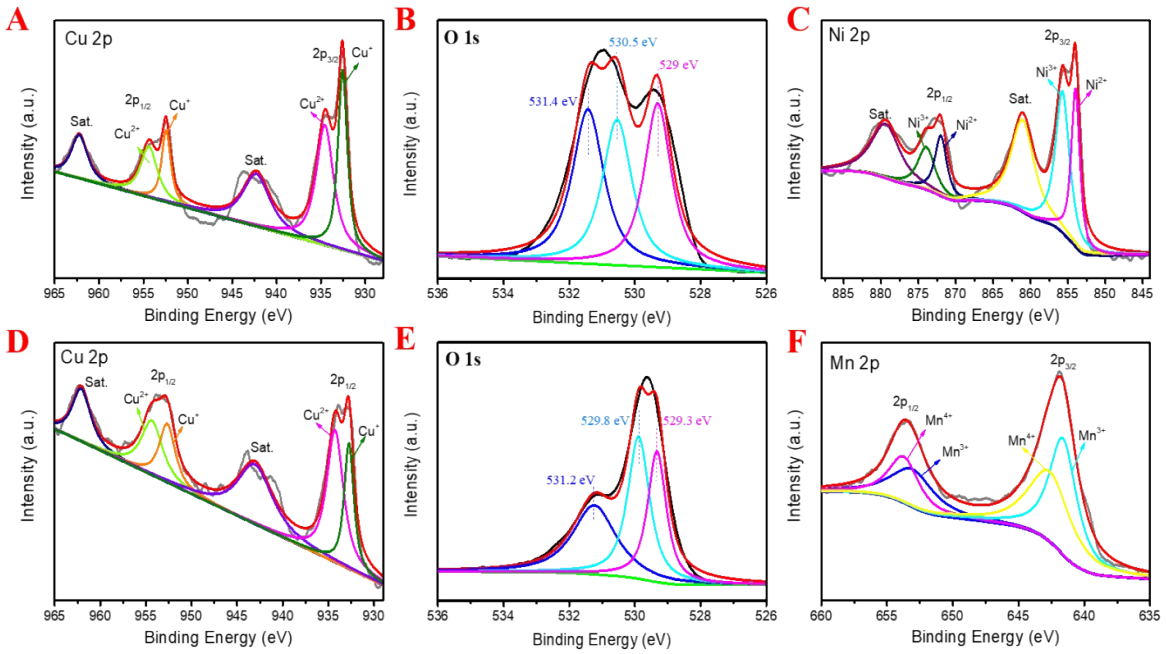

Figure S4. High-resolution XPS spectra of (A-C) CuO_x NWs@NiO: (A) Cu 2p, (B) O 1s, (C) Ni 2p, and (D-F) CuO_x NWs@MnO_x: (D) Cu 2p, (E) O 1s, (F) Mn 2p.

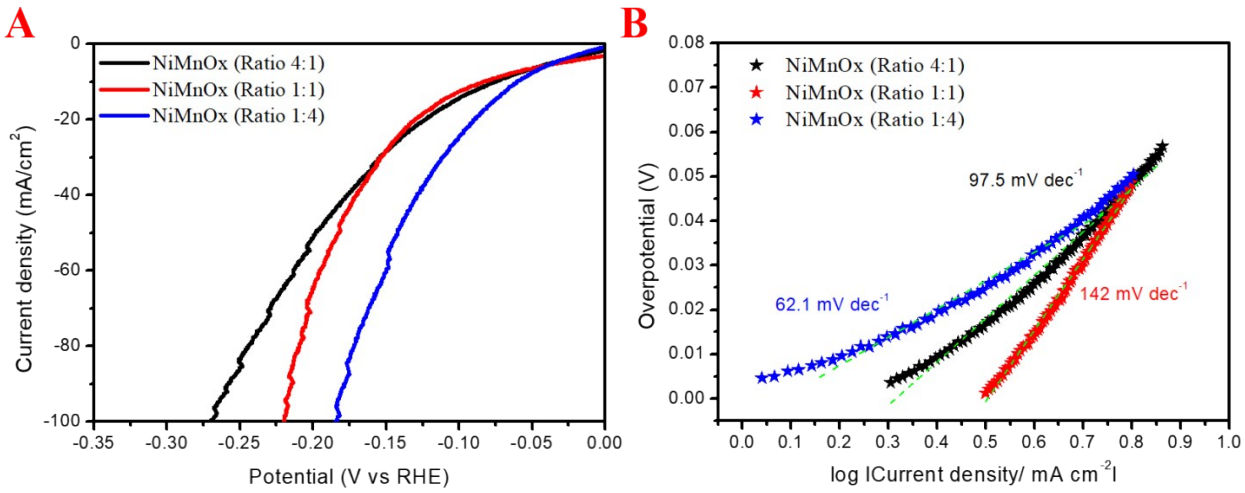

Figure S5. LSV polarization curves in 1.0 M KOH solution for HER over CuO_x NWs@$NiMnO_x$ NSs/CF electrodes prepared at different Ni/Mn ratios (4:1, 1:1 and 1:4) in the initial presursors (A) and related Tafel plots (B).

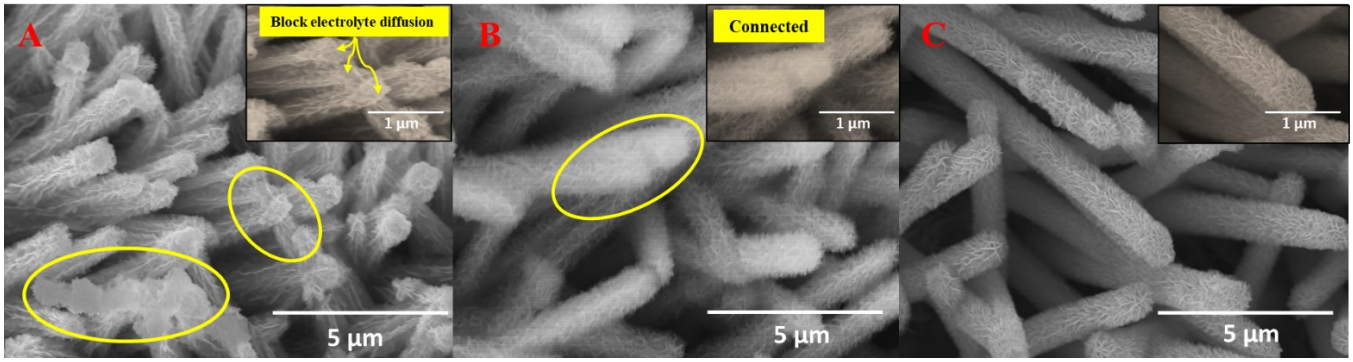

Figure S6. SEM images of CuO_x NWs@$NiMnO_x$ NSs prepared with different molar ratios of Ni:Mn in the initial presursors: (A) 4:1 (B) 1:1 (C) 1:4.

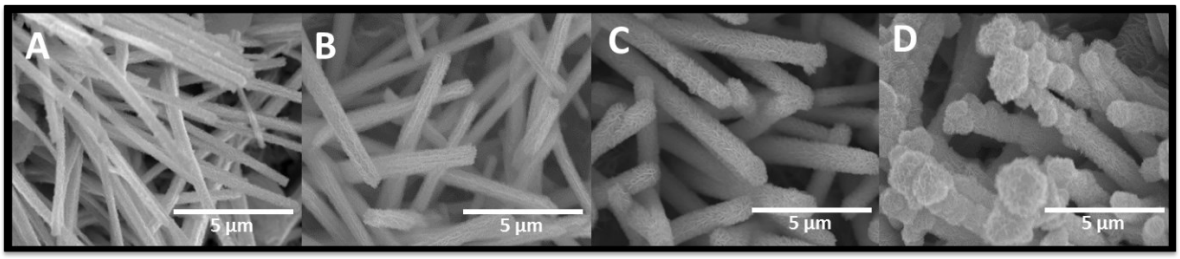

Figure S7. SEM images of CuO_x NWs@$NiMnO_x$ NSs prepared with different UPED deposition cycles: (A) 500 cycles (B) 1000 cycles (C) 1500 cycles and (D) 2000 cycles.

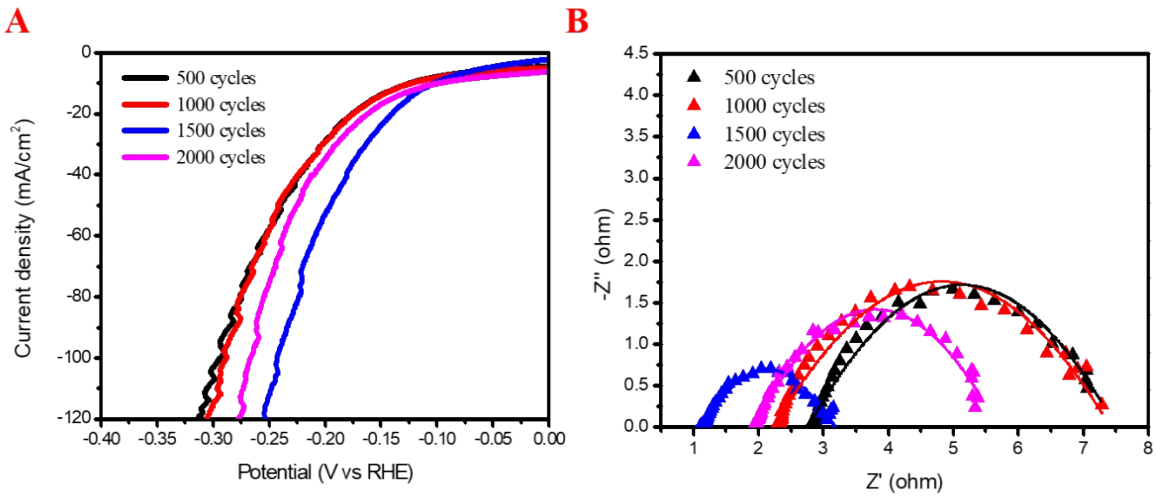

Figure S8. LSV polarization curves in the 1.0 M KOH solution for HER over CuO_x NWs@$NiMnO_x$ NSs/CF electrodes prepared with different UPED deposition cycles (500, 1000, 1500 and 2000 cycles) (A) and the related Nyquist plots at a potential of 0.2 V (B).

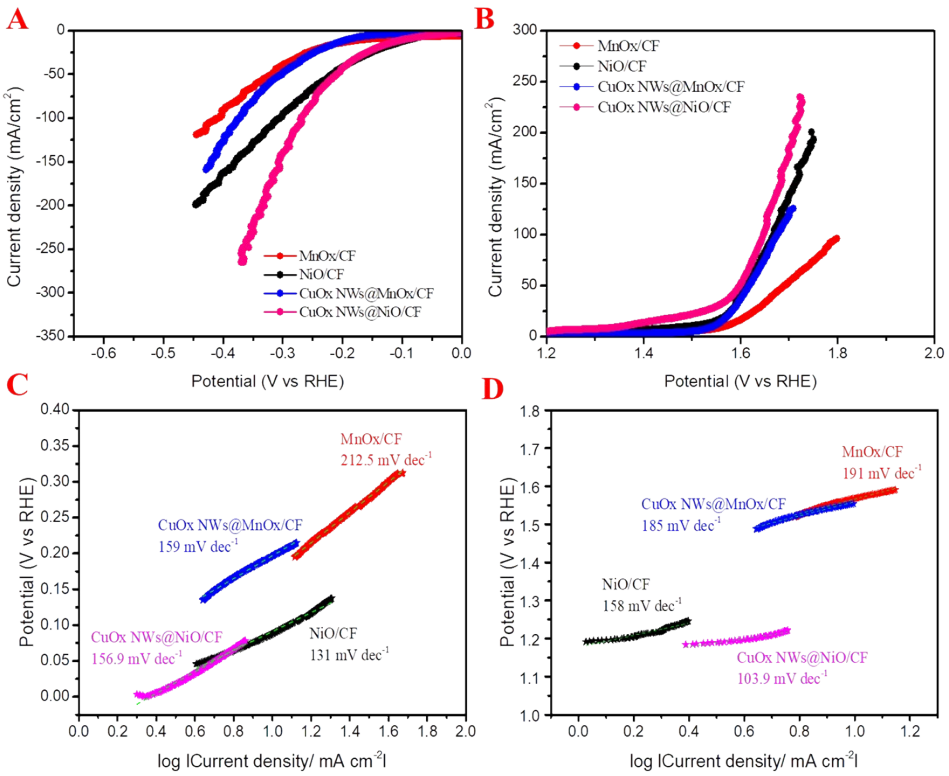

Figure S9. Water electrolysis performance of MnO_x/CF, NiO/CF, CuO_x NWs@MnO_x/CF and CuO_x NWs@NiO/CF electrodes (A-B) LSV polarization curves at a scan rate of 2 mV/s in 1.0 M KOH solution: (A) HER and (B) OER. (C-D) Tafel plots (C) HER and (D) OER.

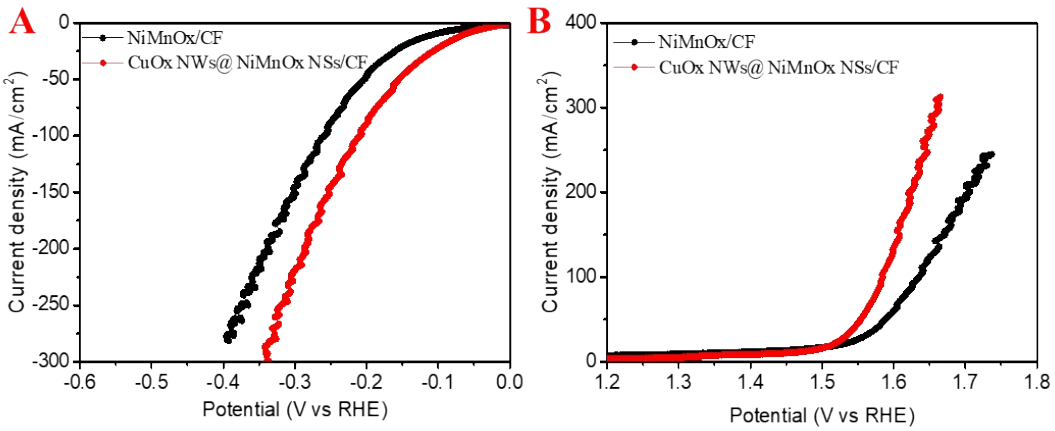

Figure S10. Comparison of LSV polarization curves over $NiMnO_x$/CF and CuO_x@ $NiMnO_x$/CF in 1.0 M KOH solution at a scan rate of 2 mV/s. (A) HER and (B) OER.

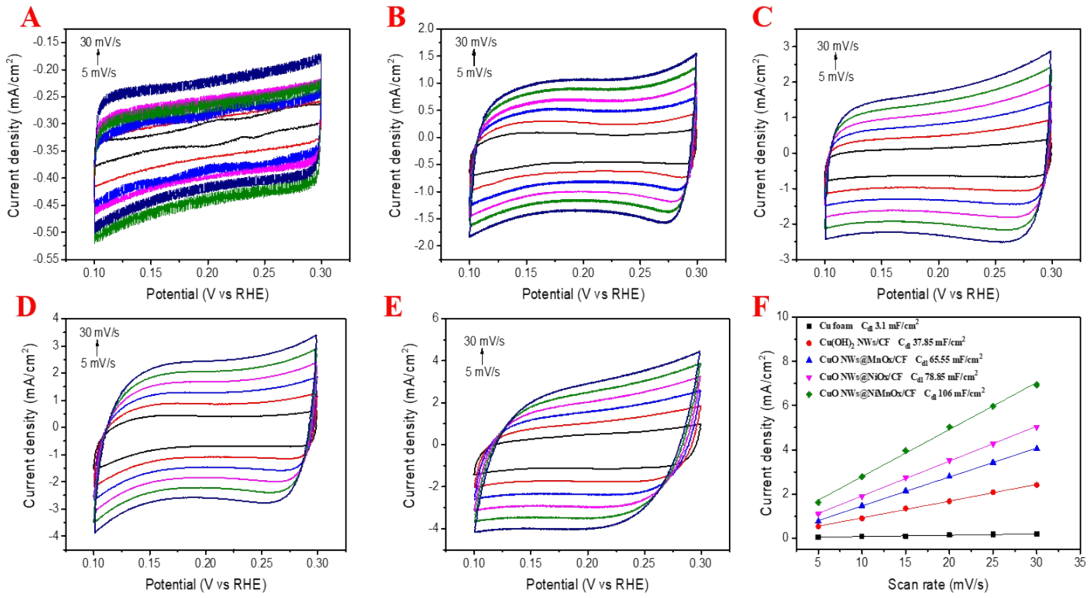

Figure S11. Cyclic voltammetry curves of (A) bare CF (CF), (B) CuO_x NWs/CF, (C) CuO_x NWs@MnO_x/CF, (D) CuO_x NWs@NiO/CF, (E) CuO_x NWs@$NiMnO_x$ NSs/CF collected between a potential range of 0.1-0.3 V (vs RHE) with scan rates of 5, 10, 15, 20, 25, 30 mV/s, respectively, in 1.0 M KOH solution. (F) Dependence of current on the scan rate at different double layer capacitances for the estimation of the electrochemical active surface area.

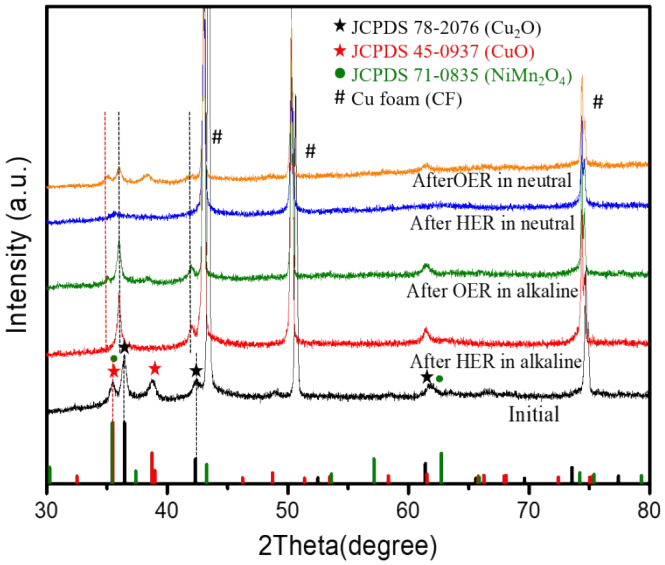

Figure S12. XRD pattern of CuO_x NWs@ $NiMnO_x$ NSs/CF after HER and OER stability test in alkaline and neutral media solution.

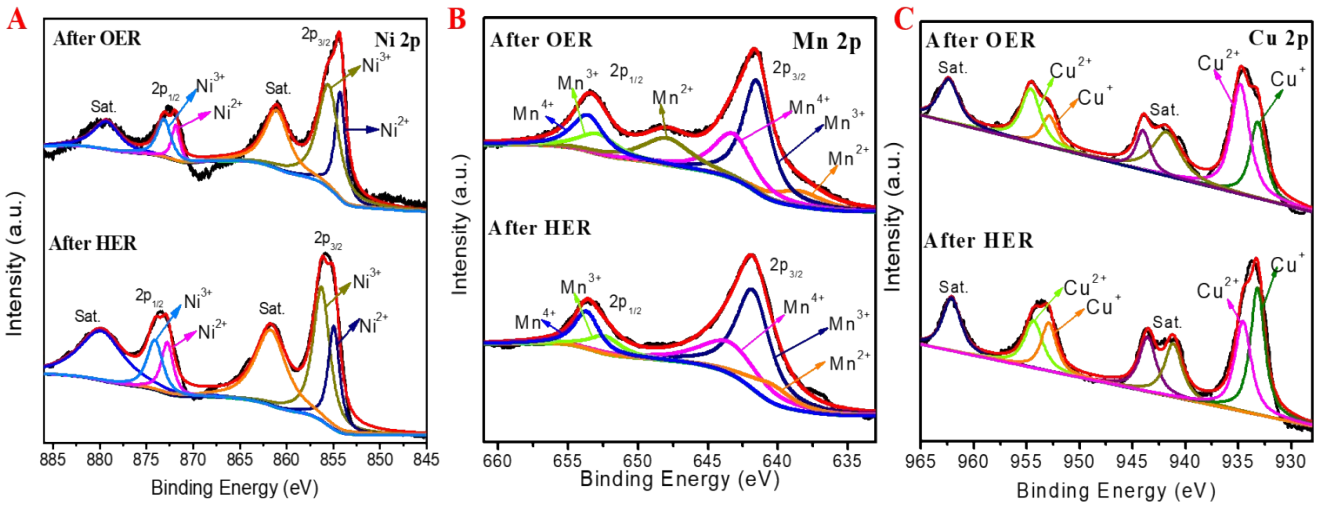

Figure S13. High-resolution XPS spectra of the CuO_x NWs@$NiMnO_x$ NSs after the stability test in the alkaline pH solutions for HER and OER: (A) Ni 2p, (B) Mn 2p and (C) Cu 2p.

Table S1. Element valence states of Ni, Mn and Cu species in the CuO_x NWs@$NiMnO_x$ NSs and their relative percentage ratio based on the deconvolution of peak areas.

Catalysts	Peak area ratio of Metal species (%)		
	$Mn^{2+}/Mn^{3+}/Mn^{4+}$	Ni^{2+}/Ni^{3+}	Cu^{+}/Cu^{2+}
After HER stability test	10.22/52.84/36.94	59.00/41.00	52.17 / 47.83
After OER stability test	23.60/43.32/33.08	48.63/51.37	35.37 / 64.63
Fresh	- / 57.16 / 42.84	39.07/ 60.93	62.78 / 37.22

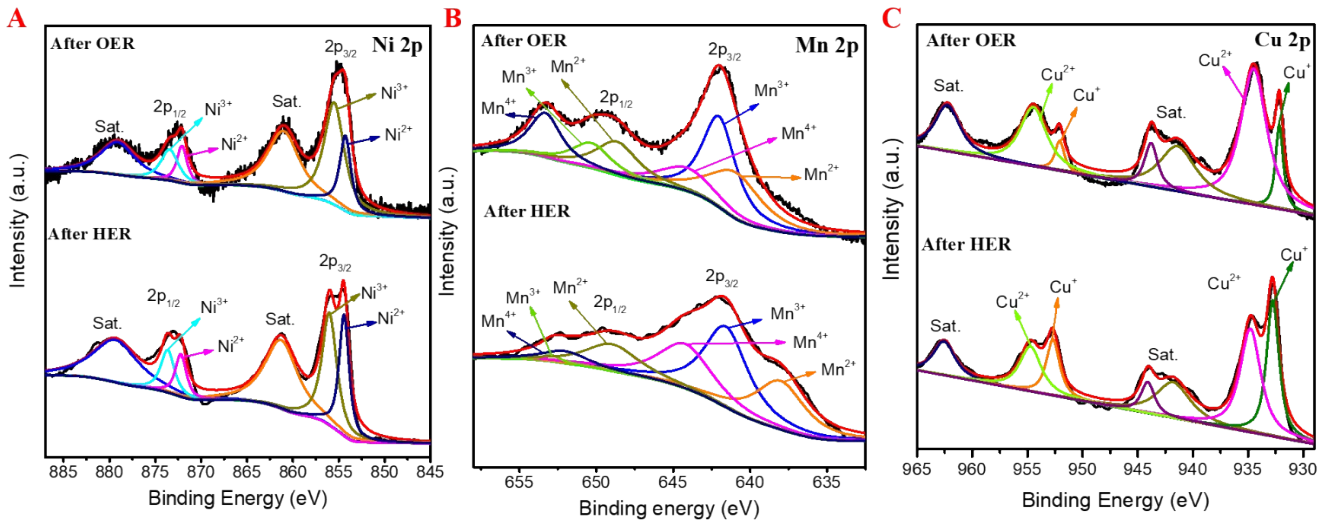

Figure S14. High-resolution XPS spectra of the CuO_x NWs@$NiMnO_x$ NSs after the stability test in the neutral pH solution for HER and OER: (A) Ni 2p, (B) Mn 2p and (C) Cu 2p.

Table S2. Element valence states of Ni, Mn and Cu species in the CuO_x NWs@$NiMnO_x$ NSs and their relative percentage ratio based on the deconvolution of peak areas.

Catalysts	Peak area ratio of metal species (%)		
	$Mn^{2+}/Mn^{3+}/Mn^{4+}$	Ni^{2+}/Ni^{3+}	Cu^{+}/Cu^{2+}
After HER stability test	34.95 / 36.74 / 28.31	42.97 /57.03	55.9 / 44.1
After OER stability test	36.02 / 38.28 / 25.70	32.39/67.61	15.32 / 84.68
Fresh	- / 57.16 / 42.84	39.07/ 60.93	62.78 / 37.22

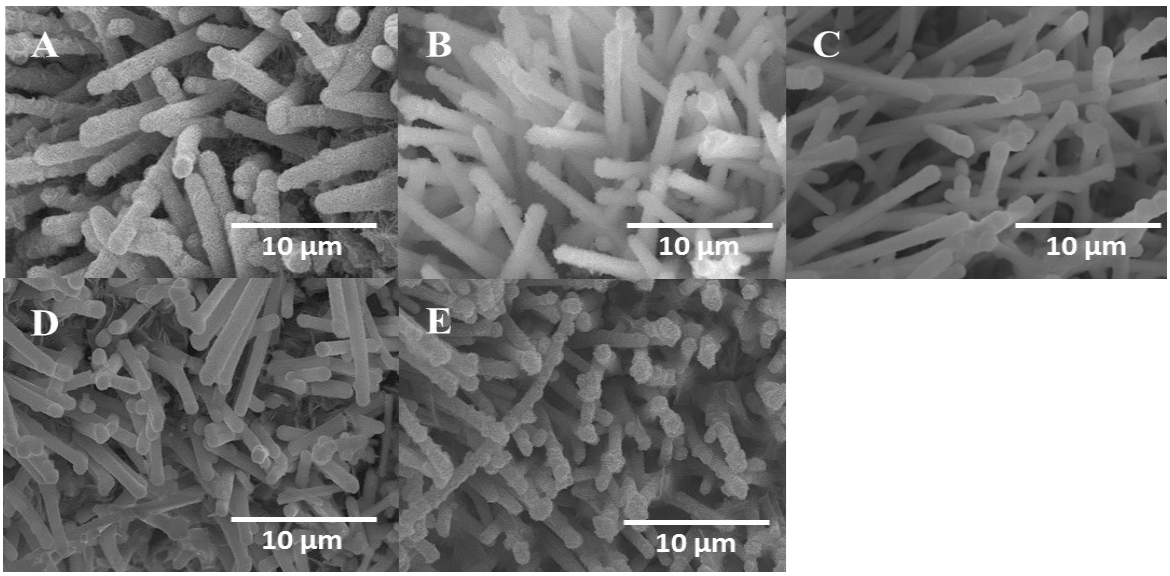

Figure S15. SEM images of CuO_x NWs@$NiMnO_x$ NSs catalysts: (A) before test; (B) after HER stability test in 1.0 M KOH solution; (C) after HER stability test in neutral PB solution; (D) after OER stability test in 1.0 M KOH solutions; and (E) after OER stability test in in neutral PB solution.

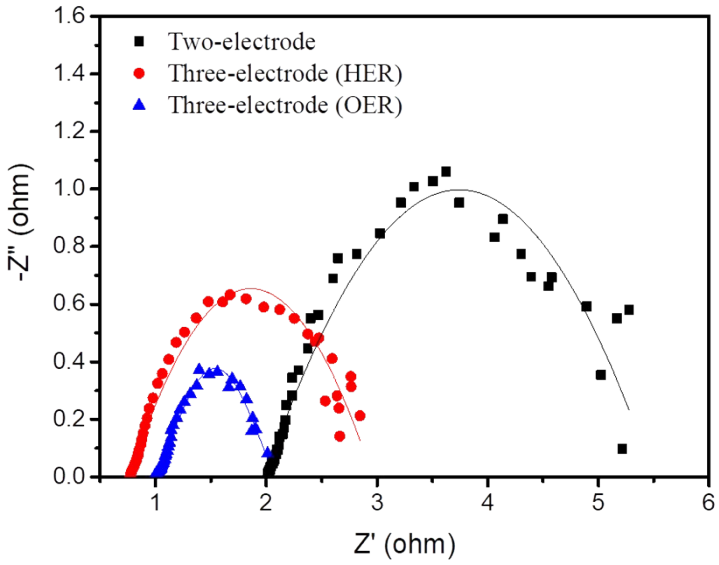

Figure S16. Comparison of Nyquist plots of CuO_x NWs@$NiMnO_x$ NSs/CF electrodes in the two-electrode system and in the three-electrode system for HER and OER in 1.0 M KOH solution.

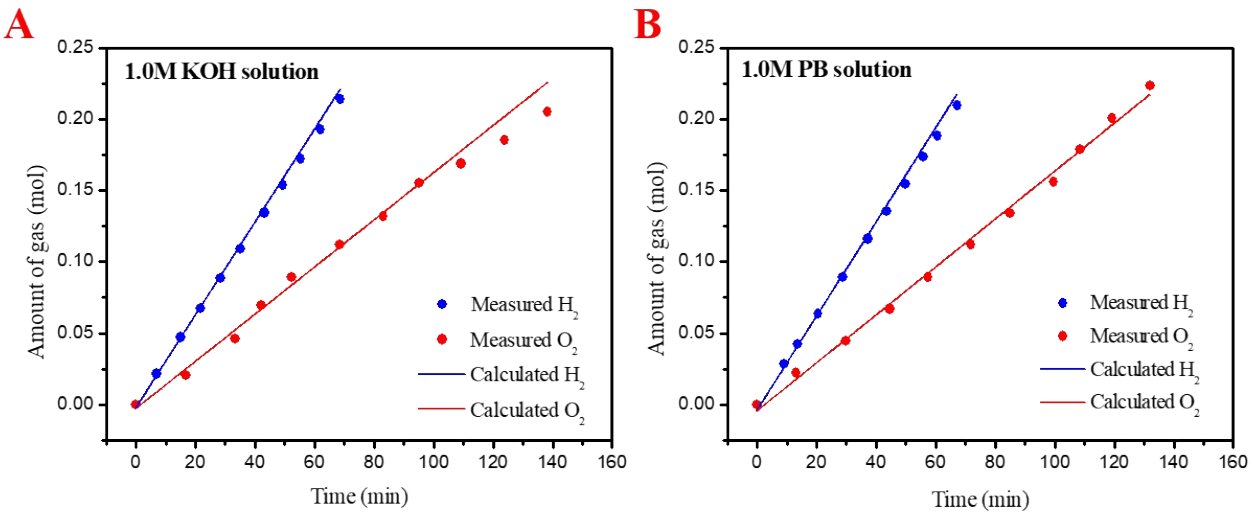

Figure S17. Theoretical hydrogen and oxygen evolution amounts vs. measured gas evolutions in 1.0 M KOH and 1.0 M PB solutions during the course of electrolysis using CuO_x NWs@$NiMnO_x$ NSs/CF electrodes in the two-electrode system for overall water electrolysis.